

Rotated echoes of molecular alignment: fractional, high order and imaginary

KANG LIN,¹ JUNYANG MA,¹ XIAOCHUN GONG,¹ QIYING SONG,¹ QINYING JI,¹ WENBIN ZHANG,¹ HANXIAO LI,¹ PEIFEN LU,¹ HUI LI,¹ HEPING ZENG,¹ JIAN WU,^{1,2} JEAN-MICHEL HARTMANN,³ OLIVIER FAUCHER,⁴ EREZ GERSHNABEL,⁵ YEHIAM PRIOR,⁵ AND ILYA SH. AVERBUKH⁵

¹State Key Laboratory of Precision Spectroscopy, East China Normal University, Shanghai 200062, China

²Collaborative Innovation Center of Extreme Optics, Shanxi University, Taiyuan, Shanxi 030006, China

³Laboratoire de Météorologie Dynamique/IPSL, CNRS, Ecole polytechnique, Université Paris-Saclay, 91128 Palaiseau, France

⁴Laboratoire Interdisciplinaire CARNOT de Bourgogne, UMR 6303 CNRS-Université Bourgogne Franche-Comté, BP 47870, 21078 Dijon, France

⁵AMOS and Department of Chemical Physics, Weizmann Institute of Science, Rehovot 76100, Israel

⁶jwu@phy.ecnu.edu.cn

⁷yehiam.prior@weizmann.ac.il

⁸ilya.averbukh@weizmann.ac.il

Abstract: We report experimental observations of rotated echoes of alignment induced by a pair of time-delayed and polarization-skewed femtosecond laser pulses interacting with an ensemble of molecular rotors. Rotated fractional echoes, rotated high order echoes and rotated imaginary echoes are directly visualized by using the technique of coincident Coulomb explosion imaging. We show that the echo phenomenon not only exhibits temporal recurrences but also spatial rotations determined by the polarization of the time-delayed second pulse. The dynamics of echo formation is well described by the laser-induced filamentation in rotational phase space. The quantum-mechanical simulation shows good agreements with the experimental results.

© 2017 Optical Society of America

OCIS codes: (320.7120) Ultrafast phenomena; (020.2649) Strong field laser physics.

References and links

1. R. W. Brown, Y.-C. N. Cheng, E. M. Haacke, M. R. Thompson, and R. Venkatesan, *Magnetic Resonance Imaging: Physical Principles and Sequence Design* (Wiley-Blackwell, 2014).
2. G. Stupakov, "Using the Beam-Echo Effect for Generation of Short-Wavelength Radiation," *Phys. Rev. Lett.* **102**, 074801 (2009).
3. D. Xiang, E. Colby, M. Dunning, S. Gilevich, C. Hast, K. Jobe, D. McCormick, J. Nelson, T. O. Raubenheimer, K. Soong, G. Stupakov, Z. Szalata, D. Walz, S. Weathersby, and M. Woodley, "Demonstration of the Echo-Enabled Harmonic Generation Technique for Short-Wavelength Seeded Free Electron Lasers," *Phys. Rev. Lett.* **105**, 114801 (2010).
4. Z. T. Zhao, D. Wang, J. H. Chen, Z. H. Chen, H. X. Deng, J. G. Ding, C. Feng, Q. Gu, M. M. Huang, T. H. Lan, Y. B. Leng, D. G. Li, G. Q. Lin, B. Liu, E. Prat, X. T. Wang, Z. S. Wang, K. R. Ye, L. Y. Yu, H. O. Zhang, J. Q. Zhang, Me. Zhang, Mi. Zhang, T. Zhang, S. P. Zhong, and Q. G. Zhou, "First lasing of an echo-enabled harmonic generation free-electron laser," *Nature Photonics* **6**, 360 (2012).
5. E. Hemsing, G. Stupakov, D. Xiang, and A. Zholents, "Beam by design: Laser manipulation of electrons in modern accelerators," *Rev. Mod. Phys.* **86**, 897 (2014).
6. E. L. Hahn, "Spin Echoes," *Phys. Rev.* **80**, 589 (1950).
7. E. L. Hahn, "Free nuclear induction," *Physics Today* **6**(11), 4 (1953).
8. N. A. Kurnit, I. D. Abella, and S. R. Hartmann, "Observation of a Photon Echo," *Phys. Rev. Lett.* **13**, 567 (1964).
9. R. W. Gould, T. M. O'Neil, and J. H. Malmberg, "Plasma Wave Echo," *Phys. Rev. Lett.* **19**, 219 (1967).
10. R. M. Hill and D. E. Kaplan, "Cyclotron Resonance Echo," *Phys. Rev. Lett.* **14**, 1062 (1965).
11. A. Bulatov, A. Kuklov, B. E. Vugmeister, and H. Rabitz, "Echo in optical lattices: Stimulated revival of breathing oscillations," *Phys. Rev. A* **57**, 3788 (1998).
12. M. Herrera, T. M. Antonsen, E. Ott, and S. Fishman, "Echoes and revival echoes in systems of anharmonically confined atoms," *Phys. Rev. A* **86**, 023613 (2012).

13. T. Meunier, S. Gleyzes, P. Maioli, A. Auffeves, G. Nogues, M. Brune, J. M. Raimond, and S. Haroche, "Rabi Oscillations Revival Induced by Time Reversal: A Test of Mesoscopic Quantum Coherence," *Phys. Rev. Lett.* **94**, 010401 (2005).
14. G. V. Stupakov, "Echo Effect In Hadron Colliders," Ssc Report SSCL- 579 (1992), <http://www.osti.gov/scitech/servlets/purl/7237216/>.
15. L. K. Spentzouris, J. -F. Ostiguy, and P. L. Colestock, "Direct Measurement of Diffusion Rates in High Energy Synchrotrons Using Longitudinal Beam Echoes," *Phys. Rev. Lett.* **76**, 620 (1996).
16. G. Karras, E. Hertz, F. Billard, B. Lavorel, J.-M. Hartmann, O. Faucher, E. Gershnabel, Y. Prior, I. Sh. Averbukh, "Orientation and Alignment Echoes," *Phys. Rev. Lett.* **114**, 15361 (2015).
17. G. Karras, E. Hertz, F. Billard, B. Lavorel, G. Siour, J.-M. Hartmann, O. Faucher, E. Gershnabel, Y. Prior, and I. Sh. Averbukh, "Experimental observation of fractional echoes," *Phys. Rev. A* **94**, 033404 (2016).
18. K. Lin, P. F. Lu, J. Y. Ma, X. C. Gong, Q. Y. Song, Q. Y. Ji, W. B. Zhang, H. P. Zeng, J. Wu, G. Karras, G. Siour, J.-M. Hartmann, O. Faucher, E. Gershnabel, Y. Prior, and I. Sh. Averbukh, "Echoes in Space and Time," *Phys. Rev. X* **6**, 041056 (2016).
19. H. Stapelfeldt, and T. Seideman, "Aligning molecules with strong laser pulses," *Rev. Mod. Phys.* **75**, 543 (2003).
20. Y. Ohshima, and H. Hasegawa, "Coherent rotational excitation by intense nonresonant laser fields," *Int. Rev. Phys. Chem.* **29**, 619 (2010).
21. S. Fleischer, Y. Khodorkovsky, E. Gershnabel, Y. Prior, and I. Sh. Averbukh, "Molecular Alignment Induced by Ultrashort Laser Pulses and Its Impact on Molecular Motion," *Isr. J. Chem.* **52**, 414 (2012).
22. M. Lemeshko, R. V. Krems, J. M. Doyle, and S. Kais, "Manipulation of molecules with electromagnetic fields," *Mol. Phys.* **111**, 1648 (2013).
23. K. Lin, Q. Y. Song, X. C. Gong, Q. Y. Ji, H. F. Pan, J. X. Ding, H. P. Zeng, J. Wu, "Visualizing molecular unidirectional rotation," *Phys. Rev. A* **92**, 013410 (2015).
24. K. Mizuse, K. Kitano, H. Hasegawa, and Y. Ohshima, "Quantum unidirectional rotation directly imaged with molecules," *Sci. Adv.* **1**, e1400185 (2015).
25. J. Parker and C. R. Jr. Stroud, "Coherence and decay of Rydberg wave packets," *Phys. Rev. Lett.* **56**, 716 (1986).
26. I. Sh. Averbukh, and N. F. Perelman, "Fractional revivals: Universality in the long-term evolution of quantum wave packets beyond the correspondence principle dynamics," *Phys. Lett. A* **139**, 449–453 (1989).
27. R. W. Robinett, "Quantum wave packet revivals," *Physics Reports* **392**, pp.1-119 (2004).
28. R. W. Boyd, "Nonlinear Optics," (Academic, 1992).
29. B. Friedrich, and D. Herschbach, "Alignment and Trapping of Molecules in Intense Laser Fields," *Phys. Rev. Lett.* **74**, 4623 (1995); "Polarization of Molecules Induced by Intense Nonresonant Laser Fields," *J. Phys. Chem.* **99**, 15 686 (1995).
30. D. Lynden-Bell, "Statistical mechanics of violent relaxation in stellar systems," *Mon. Not. R. Astr. Soc.* **136**, 101 (1967).
31. A. J. Lichtenberg, *Phase-space Dynamics of Particles* (Wiley, 1969).
32. B. Ya. Dubetskii, and V. P. Chebotaev, "Echoes in classical and quantum ensembles with determinate frequencies," *Pis'ma Zh. Eksp. Teor. Fiz.* **41**, 267 (1985) [*JETP Lett.* **41**, 328 (1985)].
33. B. Ya. Dubetskii, and V. P. Chebotaev, "Imaginary echo in a gas in a Doppler expanded transition," *Izvestiya Akademii Nauk SSSR, Seriya Fizicheskaya*, **50**, 1530 (1986) [*Bull. Acad. Sci. USSR, Phys. Ser. (English Transl.)* **50**, 70 (1986)].
34. R. Dörner, Mergel, V. Mergel, O. Jagutzki, L. Spielberger, J. Ullrich, R. Moshhammer, and H. Schmidt-Böcking, "Cold Target Recoil Ion Momentum Spectroscopy: a "momentum microscope" to view atomic collision dynamics," *Physics Reports* **330**, 95–192 (2000).
35. H. Y. Jiang, C. Y. Wu, H. Zhang, H. B. Jiang, H. Yang, and Q. H. Gong, "Alignment structures of rotational wavepacket created by two strong femtosecond laser pulses," *Opt. Express* **18**, 8990 (2010).
36. E. Hemsing, M. Dunning, B. Garcia, C. Hast, T. Raubenheimer, G. Stupakov and D. Xiang, "Echo-enabled harmonics up to the 75th order from precisely tailored electron beams," *Nat. Photonics* **10**, 512 (2016).

1. Introduction

The echo phenomenon plays an important role in many areas, ranging from modern medical technologies of magnetic resonance imaging (MRI) [1] to scientific frontiers of harmonics generation in free-electron lasers [2–5]. Since the first observation of spin echoes [6, 7] in magnetic resonance, a variety of echo phenomena were discovered in various nonlinear systems, such as photon echo [8], plasma-wave echo [9], and cyclotron echo [10]. Echoes were also found in cold atoms [11, 12], cavity QED [13], and even in particle accelerators [14, 15].

Recently, a new kind of echo phenomenon, i.e. alignment echo [16–18], was demonstrated in molecules interacting with laser fields. A series of alignment events (for a review of laser-induced alignment, see [19–22]) spaced with regular time intervals were first detected by measuring

the laser-induced birefringence of a molecular gas sample subject to a pair of time-delayed ultrashort laser pulses [16]. Fractional alignment echoes at rational fractions of the time delay between the pump pulses were predicted [16] and the lowest-order one (1/2) was observed via the third-harmonic generation in a room-temperature gas of CO₂ molecules [17]. Higher order fractional echoes are difficult to be probed optically due to the low efficiency of the high order harmonic generation required for their detection. We overcame the difficulty by directly imaging the molecular axis angular distribution from the measured ion fragments produced by the ultrafast Coulomb explosion of multiply ionized molecules [23, 24]. Besides the fractional echoes of various orders, two new kinds of alignment echoes, namely rotated and imaginary alignment echoes were theoretically and experimentally studied in [18]. For the case when the polarization of the second pulse makes a cross angle β with respect to that of the first one, the primary echo shows spatial recurrence at 2β , thus forming the rotated echo of molecular alignment. Normally, echoes are supposed to appear after the excitation by the second pulse. However, by "reversing" the dynamics to negative times, echoes are expected at times before the second pulse. Despite the impossibility of reaching negative times in the real world, we successfully demonstrated [18] the existence of imaginary alignment echo by focusing the observation around the full quantum revival [25–27] of the alignment induced by the second laser pulse. The dynamics in the time region just before the revival is equivalent to the post-second-pulse dynamics analytically continued to negative times.

In this paper, we report an experimental observation of the rotated fractional echoes, rotated high order echoes and rotated imaginary echoes in a molecular beam of N₂O. The spatiotemporal evolution of the molecular angular distribution is directly measured via the technique of coincident Coulomb explosion imaging [23]. In what follows, we will start with the theoretical analysis of the rotated echo formation using a simple 2D model. A detailed description of the experimental setup and data analysis is given afterwards. We further reproduce the experimental results by quantum-mechanical simulations, which agree well with the experimental observations.

2. Rotational phase space analysis

To get the physical insight, we start with a theoretical analysis of the rotational dynamics of an ensemble of 2D linear molecular rotors. The molecules initially have an isotropic angular distribution, and a Gaussian distribution with spread (σ) in angular velocity ω [16–18]. The linearly polarized laser field drives the molecular rotation by an interaction potential of $V(\phi, t) = -(\Delta\alpha/4)E^2(t)\cos^2\phi$ [28, 29], where ϕ is the angle between the laser polarization and the molecular axis, $\Delta\alpha$ is the polarizability anisotropy of the molecule and $E(t)$ is the temporal envelope of the laser pulse. An impulsive kick forces the molecular axis to rotate towards the polarization direction of the laser pulse, leading to a transient alignment along this direction shortly after the kick. The alignment factor $\langle\cos^2\phi\rangle$ is used to characterize the alignment degree of the ensemble. In our case of 2D free rotors, the mean value of $\langle\cos^2\phi\rangle = 0.5$ indicates an isotropic distribution of molecular orientations, while $\langle\cos^2\phi\rangle$ is larger or smaller than 0.5 for alignment and anti-alignment, respectively. After the excitation by the short laser pulse, the field-free evolutions of the angle ϕ of the molecular axis and of the angular velocity ω are described by: $\phi = \phi_0 + \omega t$, $\omega = \omega_0 - \Omega \sin(2\phi_0)$, where ω_0, ϕ_0 are the initial conditions, and Ω is proportional to the intensity of the kick.

As detailed in [16–18], the probability distribution of the molecular axis in phase space after the impulsive kick is given by:

$$f(\omega, \phi, t) = \frac{1}{2\pi} \frac{1}{\sqrt{2\pi}\sigma} \exp\left[-\frac{[\omega - \Omega \sin(2\omega t - 2\phi)]^2}{2\sigma^2}\right]. \quad (1)$$

The initial phase-space distribution is shown in Fig. 1(a), as mentioned above, with an isotropic angular distribution (horizontal axis) and a Gaussian angular velocity distribution (vertical axis).

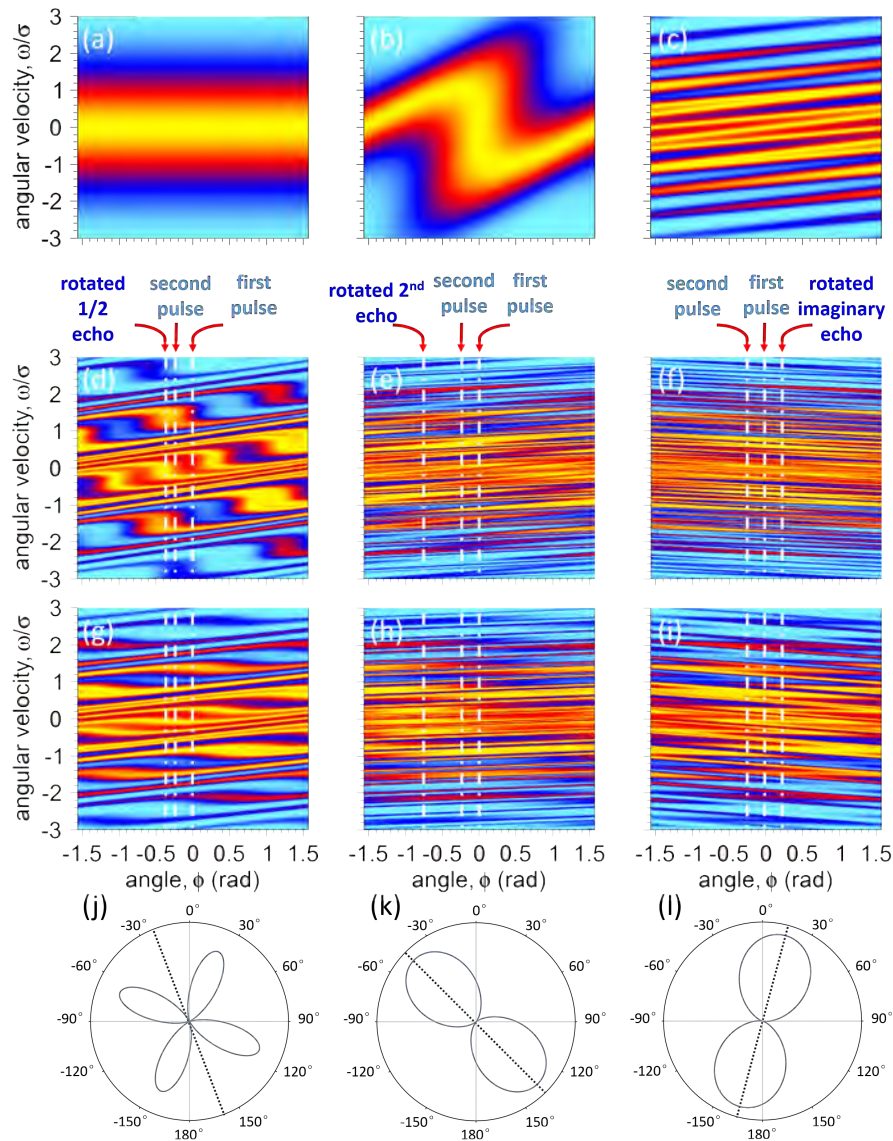


Fig. 1. Rotated echo formation. The first pulse is applied at $t = 0$, $\phi = 0$, with $\Omega_1/\sigma = 1$. The second pulse is applied at $t = T$ (such that $\sigma T = 5$), at crossing angle $\beta = -\pi/12$ with respect to the first pulse, (a)-(c) Laser-induced filamentation of the phase-space density distributions. (a) Initial phase-space density distribution. (b) Folding and alignment shortly after the first pulse at $t = 0.1T$. (c) Filamentation at $t = T$ after the first pulse. (d)-(f) Rotated echo formation after the second pulse, $\Omega_2/\Omega_1 = 0.333$. The polarization angles of the first and the second pulses, as well as the rotation angles of echoes at different times are indicated by the white dashed lines. (d) Rotated 1/2 fractional echo at $(t, \phi) = (1.46T, 1.5\beta)$. (e) Rotated second order echo at $(t, \phi) = (2.82T, 3\beta)$. (f) Rotated imaginary echo at $(t, \phi) = (-1.2T, -\beta)$. (g)-(i) Rotated echo formation after the second pulse, $\Omega_2/\Omega_1 = 0.16$ (close to the value used in our experiments). (g) Rotated 1/2 fractional echo at $(t, \phi) = (1.533T, 1.5\beta)$. (h) Rotated second order echo at $(t, \phi) = (3.13T, 3\beta)$. (i) Rotated imaginary echo at $(t, \phi) = (-0.865T, -\beta)$. (j)-(l) are the corresponding polar plots of the angular distributions for (g)-(i), respectively. A constant angular-independent background was subtracted in these polar plots. The theoretically expected directions of the rotated echoes are indicated by the gray dashed lines.

The short kick imparts rotation of molecules with angular speed $-\Omega \sin(2\phi_0)$ while not moving them during the interaction. Immediately after the kick, the phase-space distribution starts folding towards the polarization direction of the excitation pulse, i.e. $\phi = 0^\circ$. With course of time, a symmetric folded pattern corresponding to the laser-induced alignment appears shortly after the kick, as shown in Fig. 1(b). At longer times, the phase-space probability distribution develops multiple parallel filaments due to dispersion in angular velocities, as shown in Fig. 1(c), and the alignment factor $\langle \cos^2 \phi \rangle(t)$ takes the isotropic value of 0.5. Since the phase-space volume is constant, the width of each filament narrows with the number of these filaments growing, till they become almost horizontal and uniform in density. The neighboring filaments are separated in angular velocity by $\sim \pi/t$, as can be seen from Eq. (1). Such a filamentation of phase space is well known in stellar systems [30] and in accelerator physics [31], and the folding of the phase-space distribution shown in Fig. 1(b) has much in common with the bunching effect observed in particle accelerators beams [14, 15].

When a second kick is applied (at $t = T$) polarized at angle β with respect to the first one, it will fold each filament in a way similar to Fig. 1(b), which is not shown here. However, the initial position of the folded features will be at $(\phi, \omega) = (\beta, m\pi/T + \beta/T)$, where m is the filament number. Due to the "quantization" of the angular velocities, the folded parts of the filaments will bunch up after another delay T (i.e. near $t = 2T$) at the angular position $\phi = 2\beta$, resulting in an echo not only delayed in time, but also rotated by an additional angle β with respect to the second pulse, or 2β with respect to the first one [18]. More generally, the rotation angle of echoes observed at time $t > T$ after the first pulse is given by:

$$\phi = \beta + [(m\pi/T + \beta/T)](t - T)(\text{mod } \pi). \quad (2)$$

Hence, for echoes appearing at $t = T + (k/n)T$, the rotation angle is given by $\phi = \beta + (m\pi + \beta)(k/n)(\text{mod } \pi)$, where k and n are integers. The 1st order rotated echo was discussed in [18] for $n = 1, k = 1$. Here, we focus on the high order echoes of $n = 1, k > 1$, appearing at $(t, \phi) = (3T, 3\beta), (4T, 4\beta), \text{etc.}$ Figures 1(e) and 1(h) show the phase-space distributions of the 2nd order rotated echo for different intensity ratios between the two excitation pulses, i.e. I_2/I_1 . The folding effect is sensitive to the intensity ratio of I_2/I_1 . As illustrated in [16, 18], the echo signal can be optimized by changing the relative strength between the two pulses. For $n > 1$, the equation describes the fractional echoes appearing at rotational fractions of the time delay T . Figures 1(d) and 1(g) show the rotated 1/2 fractional echo ($n=2$) that happens at $(t, \phi) = (1.5T, 1.5\beta)$. By integrating over the angular velocity in phase space, i.e. projecting the 2D filament density distribution in Figs. 1(g) and 1(h) to the horizontal axis (angular dimension), one can extract the angular distribution of the molecular ensemble, as shown in the polar plots in Figs. 1(j) and 1(k) correspondingly.

The above analysis addresses rotated echoes appearing after the excitation of the second pulse. As discussed in [18], counter-intuitive imaginary echoes [32, 33] may show up before the second pulse if the rotational dynamics is analytically continued to negative times. The imaginary alignment echoes can be observed by utilizing the phenomenon of quantum revivals [25–27] as a mechanism for time reversal. Here, we predict the appearance of rotated imaginary echo at $(-T, -\beta)$ [Figs. 1(f), 1(i) and 1(l)] in a similar manner and report its experimental observation for the first time. The reversed rotation direction of the echo further confirms our time reversal explanation of the mechanism responsible for the imaginary echo formation.

3. Experimental setup

We create the rotated alignment echoes in a supersonic molecular beam of N_2O driven by a pair of time-delayed and polarization-rotated femtosecond laser pulses, denoted as P_1 and P_2 respectively. A schematic diagram of the experimental setup is shown in Fig. 2. The time delay between P_1 and P_2 is controlled by a motorized delay stage in the arm of P_1 . Two half-wave

plates are inserted in each of the two arms to set the polarization of P_1 along the Z-axis and adjust the polarization direction of P_2 . An intense, circularly polarized probe pulse is used to Coulomb-explode the excited molecules at various time delays, generating an image from which the molecular orientation at that time can be derived. The laser pulses are delivered from a multipass amplifier Ti:sapphire laser system (10KHz, 25fs, 790nm), and are collinearly focused in the supersonic gas jet of N_2O by a concave silver mirror ($f = 7.5\text{cm}$) inside the ultrahigh vacuum chamber of a COLTRIMS (COLd Target Recoil Ion Momentum Spectroscopy) apparatus [34]. By measuring the time-delay-dependent single ionization yield as a cross-correlation between every two pulses, we estimate the pulse duration in the interaction region to be about 60 fs. The peak intensities of P_1 , P_2 and the probe pulse are measured to be $I_1 \sim 5.0 \times 10^{13} \text{ W/cm}^2$, $I_2 \sim 0.8 \times 10^{13} \text{ W/cm}^2$, and $I_{\text{probe}} \sim 4 \times 10^{14} \text{ W/cm}^2$, respectively. The rotational temperature of the supersonic molecular beam can be estimated from the translation temperature, which can be derived from $T_{\text{trans}} = \Delta p^2 / [4 \ln(4) k_B M]$, where k_B is the Boltzmann constant, Δp and M are the full width at half maximum (FWHM) of the momentum distribution (in the jet direction, i.e. Y-axis) and the mass of the singly ionized N_2O^+ , respectively. In our experiment we measure a momentum width in the jet direction of $\Delta p \sim 10.2 \text{ a.u.}$ of N_2O^+ ions created by the laser pulse polarized along Z-axis, thus we assume that the upper limit of the rotational temperature is $\sim 75\text{K}$.

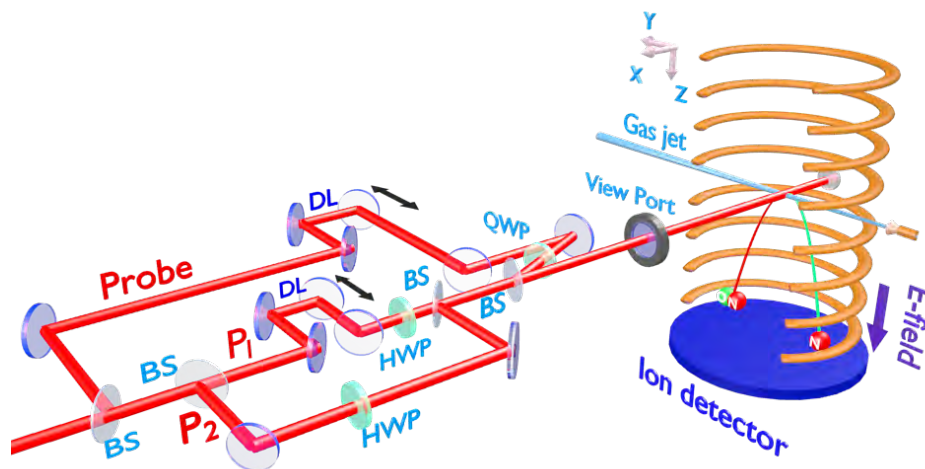


Fig. 2. Experimental setup. Two linearly polarized pump pulses P_1 and P_2 are employed to stimulate molecular alignment echoes of N_2O . An intense circularly polarized probe pulse is used to trace the molecular angular distribution at various times. The measurement is performed in a reaction microscope of COLTRIMS. BS, beam splitter; HWP, zero-order half wave plate; QWP, zero-order quarter wave plate; DL, delay line.

The fragment ions are guided by a weak homogeneous static electric field ($\sim 22.3 \text{ V/cm}$) to a time- and position-sensitive detector at the end of the spectrometer, consisting of a two-layers stack of microchannel plates and a delay-line detector. The three dimensional momenta of the fragment ions can be retrieved from the measured times of flight and positions of impact. Since the Coulomb explosion is much faster than the molecular rotational period, the instantaneous orientation of the molecular axis at the time of ionization can be reconstructed from the relative momenta of the coincidentally measured ion pair. By scanning the arrival time of the probe pulse, snapshots of the molecular angular distribution at various times directly visualize the molecular rotational motion.

4. Experimental results

Several constraints define the temporal condition for experimental observation of high order echoes, which imposes the use of a relatively long time window for the measurement. This requirement conflicts with the appearance of fractional quantum rotational revivals [25–27] at earlier times of the molecular alignment. To avoid such a temporal overlap, the experiments reported here were performed with N_2O molecules. The rotational full revival time of this molecule is 39.9 ps [35], but unlike CO_2 (used in our earlier studies [16–18]), due to the symmetric weight of odd and even nuclear spin states, the field-free evolution of N_2O does not exhibit quarter revivals, thus providing a clear time window of approximately 20 ps for the manipulation and observation of the alignment echoes. The Coulomb explosion double ionization channel, i.e., $N_2O + n\hbar\omega \rightarrow NO^+ + N^+ + 2e$, is employed to retrieve the orientation of molecular axis and since the molecules are mostly fragmented in the polarization plane of the probe pulse, we restrict the data analysis in this plane by selecting molecules confined to $[-20^\circ, 20^\circ]$ with respect to the Y-Z plane.

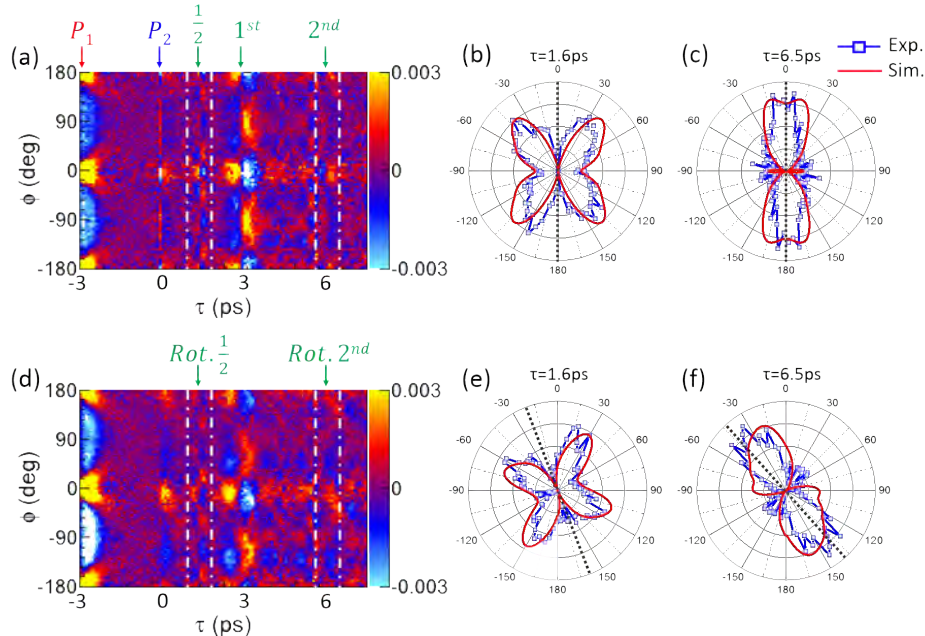


Fig. 3. Experimentally measured time-dependent angular distribution of (a) the $1/2$ fractional, the full and the 2^{nd} order echoes, and (d) the rotated $1/2$ fractional, the rotated full, and the rotated 2^{nd} order echoes of N_2O . In both cases the echo region is highlighted between the vertical dashed white lines. The corresponding polar plots of the angular distributions are shown in (b)-(c) and (e)-(f). The angular-independent negative background was subtracted in these polar plots. (b) and (c) for the $1/2$ and 2^{nd} order echoes, and (e) and (f) for the rotated $1/2$ and 2^{nd} order echoes. The red solid lines in (b)-(c) and (e)-(f) are the results of quantum simulations, which agree well with the experiments. The theoretically expected directions of echoes and the rotated ones are indicated by the gray dashed lines.

The measured time-dependent angular distribution is shown in Fig. 3(a), where τ is the time delay of the probe pulse with respect to P_2 , and ϕ is the azimuth angle between the molecular axis and the polarization direction of P_1 in the Y-Z plane. In order to eliminate the imperfection of the circularity of the probe pulse and to enhance the visibility, the total probability of the angular distribution at each time step is normalized to unity, i.e. the integrated Coulomb explosion signal

over $[-180^\circ, 180^\circ]$ for each slice is normalized to 1, and the averaged angular distribution between P_1 and P_2 is subtracted. The time delay between P_1 and P_2 is set to 3 ps. To enhance the visibility of the weak 2^{nd} order echo, we zoom the color-bar scale which saturates the negative maximum of the signal around $\tau = -3$ ps and 3 ps, as featured in white color. As shown in Fig. 3(a), shortly after the kick of P_1 at $\tau = -3$ ps, the molecular angular distribution is centered around $\phi = 0^\circ (\pm 180^\circ)$, corresponding to alignment along the polarization direction of P_1 , but disperses quickly due to the spread in angular velocities of the molecular rotors. The second pulse with polarization parallel to the first one ($\phi = 0^\circ$) is applied at $\tau = 0$ ps. Instantaneous alignment is created, followed by the appearance of the 1/2 fractional and full echoes around $\tau = 1.5$ ps and 3 ps respectively. Following the first full echo, higher order echoes appear at multiple integers of the time delay, namely at $\tau = 6$ ps, 9 ps, etc, in this case. Since the magnitude of echoes rapidly decreases with their order, only the lowest order one, i.e. the 2^{nd} order echo at $\tau = 6$ ps, is clearly observed (between the white dashed lines) in Fig. 3(a). As we have already demonstrated [18], the first order full echo depicts a rapid transition from alignment to anti-alignment. However, here we find that the 2^{nd} order echo exhibits the reverse order - a transition from anti-alignment to alignment. The polar plot of the angular distribution of the 2^{nd} order echo in the alignment region at $\tau = 6.5$ ps is depicted in Fig. 3(c). Since the 1/2 fractional echo shows a butterfly shaped distribution [Fig. 3(b)], we take the vertical axis of symmetry along $\phi = 0^\circ$ to indicate the alignment direction of reference, as shown in gray dashed line in Fig. 3(b). Our quantum-mechanical simulation shows good agreements with the experimental observations of both 1/2 and 2^{nd} order echoes, as shown by the red curves in Figs. 3(b) and 3(c). The quantum mechanical calculation was carried out by numerically solving the time-dependent Schrödinger equation, and the alignment echo was successfully reproduced. The angular-distribution-probability for each initial molecular rotational state was calculated separately as a function of time, and later integrated according to the initial Boltzmann distribution and proper spin statistics. For details of this quantum mechanical simulation see [18]. It should be noted that while the direct observation of higher order echoes by optical means is possible by observing the laser-induced birefringence [16], here we demonstrate direct access to the angular distribution enabled by the coincident Coulomb explosion imaging [18, 23].

We have previously shown [18] that when the polarization of the second pulse is not parallel to that of the first one, i.e. there is a cross angle $\beta \neq 0^\circ$ between them, the primary echo shows an angular response at 2β . According to Eq. (2), not only the primary echo, but also the fractional and the high order echoes will exhibit the same properties of rotated angles of the molecular alignment. To observe the rotated high order echoes, we repeat the experiment described above by rotating the polarization direction of P_2 by $\beta = -14^\circ$ with respect to P_1 . As shown in Fig. 3(d), the rotated 1/2 fractional echo, the rotated full echo, and the rotated 2^{nd} order echo after P_2 are observed. Here we focus on the rotated 1/2 fractional echo and the rotated 2^{nd} order echo only, for more details of rotated full echo, see [18]. Since P_2 is applied at -14° , the instantaneous alignment induced by P_2 already shows angular alignment centered around this angle. As expected from Eq. (2), the rotated 1/2 fractional echo and the rotated 2^{nd} order echo generate angular distributions centered around $\phi = -21^\circ$ and $\phi = -42^\circ$, corresponding to 1.5β and 3β respectively, as shown in Figs. 3(e) and 3(f), which exactly correspond to the theoretical prediction of Figs. 1(j) and 1(k) respectively.

A different regime that had been explored before is the domain of negative times [18]. By propagating the rotational dynamics to negative times, an imaginary echo is predicted to appear before P_2 . Since this is not physically possible, the effect has been demonstrated by utilizing the phenomenon of quantum revival [25–27]. Within the framework of the 2D classical model considered in Sec. 2, the imaginary echo rotated in the opposite direction [see Figs. 1(f), 1(i) and 1(l)] compared to the "regular" echoes. To experimentally verify this point, we looked at the time window before and around the full quantum revival of the alignment response induced by the second pulse. Figures 4(a) and 4(b) show the measured angular distribution and alignment

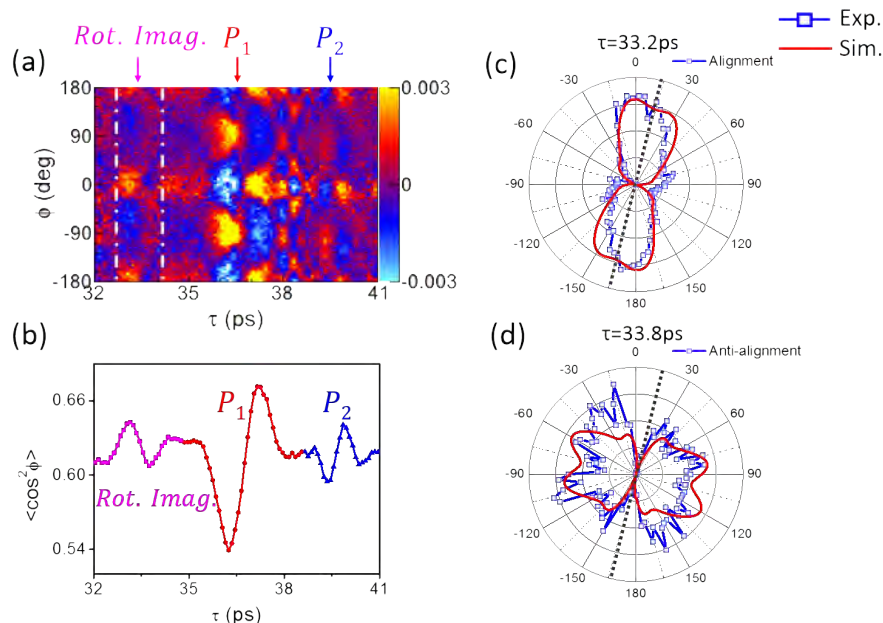


Fig. 4. (a) Time-dependent angular distribution of rotated imaginary echo. (b) The measured alignment factor as a function of probe time delay. The red and blue curves show the full revivals of the alignment induced by P_1 and P_2 respectively. The rotated imaginary echo is presented by the magenta curve. (c) and (d) are the polar plots of the angular distributions of the rotated imaginary echoes at alignment and anti-alignment times respectively, where the angular-independent negative background was subtracted. The red curves in (c) and (d) are quantum simulations. The theoretically expected directions of the rotated echoes are indicated by the gray dashed lines.

factor as a function of the probe time delay around the time of full revivals of the alignment created by P_1 and P_2 applied at $\tau = -3$ ps and $\tau = 0$ ps, respectively. As depicted in magenta in Fig. 4(b), a significant alignment signal is observed around $\tau = 33.2$ ps, i.e., 6 ps before the full revival of the alignment created by P_2 (blue curve). The imaginary echo exhibits a transition from anti-alignment to alignment. The associated angular distributions of alignment and anti-alignment are shown in polar plots in Figs. 4(c) and 4(d), respectively. As expected from time reversal, both alignment and anti-alignment rotate in the clockwise direction and are centered around $\phi = 14^\circ$ and $\phi = 104^\circ$, respectively, in agreement with the prediction of a rotated imaginary echo, as shown in Fig. 1(l) for the alignment. The quantum simulations (red solid curves) in Figs. 4(c) and 4(d) agree well with the experimental observations.

5. Conclusion

In conclusion, we experimentally observe various rotated echoes of molecular alignment, including rotated fractional echo, rotated high order echo and rotated imaginary echo. A pair of time-delayed and polarization-skewed pump pulses are employed to stimulate the rotated echoes in a molecular beam of N_2O . Direct access to the molecular angular distribution is achieved by scanning the time delay of a circularly polarized probe pulse by using the technique of coincident Coulomb explosion imaging. The rotated echoes are well explained using a classical analysis of laser-induced filamentation in rotational phase space. The spatiotemporal properties of the rotated echoes provide opportunities to control the echoes by varying the arrival time and polarization

of the second pulse. The common properties shared by echo phenomena in various systems may be beneficial to related fields, such as the echo-enabled harmonics generation (EEHG) in free-electron lasers [36].

Funding

National Natural Science Fund of China (NSFC) (11425416, 11374103, 61690224, 11621404); 111 Project of China (B12024); Conseil Régional de Bourgogne (PARI program), CNRS, French National Research Agency (ANR) through the CoConicS program (contract ANR-13-BS08-0013); Labex ACTION program (contract ANR-11-LABX-0001-01); Israel Science Foundation (Grant No. 746/15); ICORE program "Circle of Light"; Minerva Foundation.

Acknowledgments

I. A. acknowledges support as the Patricia Elman Bildner Professorial Chair. This research was made possible in part by the historic generosity of the Harold Perlman Family. K. L. acknowledges the support from Outstanding doctoral dissertation cultivation plan of action (YB2016037) of ECNU.